Oxygen gradients for open well cellular cultures *via* microfluidic substrates†

Joe F. Lo, Elly Sinkala and David T. Eddington*

Received 25th March 2010, Accepted 28th May 2010
DOI: 10.1039/c004660d

Controlling oxygen concentration at a microscale level can benefit experimental investigations involving oxidative stress, ischemia, and reactive oxygen species (ROS) mediated cellular pathways. Here, we report the application of microfluidic gradient generation in an open-well culture model, in which a gradient of gas is delivered *via* diffusion through a gas permeable substrate that separates cells from the gas microchannels below. By using diffusion to localize oxygen delivery, microgradients of oxygen concentrations can be rapidly and controllably applied without exposing cells to mechanical stresses or reducing culture volumes inside microfluidic culture chambers. Furthermore, we demonstrate the modulation of intracellular ROS levels in Madin–Darby Canine Kidney (MDCK) cells by applying these oxygen microgradients. Increases in ROS levels consistent with both oxidative stress and hypoxic exposures were observed in MDCK cells. The measured ROS increases were comparable to 100 μM hydrogen peroxide exposure in a control comparison, which is within the range of standard ROS induction methods. Incubation with 200 μM vitamin C was able to demodulate the ROS response at both hypoxic and hyperoxic exposures. By providing microfluidic controlled gradients, constant ROS exposure, and a shear-free open well design, the devices introduced here greatly improve upon standard oxygen-based culturing methods.

1. Introduction

Molecular oxygen is critical in many cellular pathways involving careful homeostatic balance in order to maintain growth, proliferation, and controlled cell death. Low oxygen (hypoxic) levels influence tumor metastasis[1] while high oxygen (hyperoxic) levels exert both wound healing[2,3] and cytotoxic effects.[4] Oxygen levels regulate the degradation of the hypoxia inducible factor 1-alpha (HIF-1α), which is a global transcription factor implicated in many signaling pathways.[5] In addition, reactive oxygen species (ROS) are signaling molecules involved in both hyperoxic and hypoxic pathways and are correlated to the local oxygen environment. For instance, ROS is implicated in stabilizing HIF-1α during hypoxia,[6] as well as in providing deleterious radicals in inflammatory and hyperoxic conditions.[7–9] Because these oxidative mechanisms overlap both hypoxic and hyperoxic regimes, a gradient-based assay is required to probe oxygen as a controlled and dose-dependent variable. To illustrate such an assay, we applied oxygen microgradients to systematically modulate the ROS levels in a cell culture-based platform without using exogenous chemicals such as hydrogen peroxide, which is the current gold standard for these types of applications. This gradient-based approach enables new experimental protocols previously impossible or very difficult to implement with standard cell culture methods.

Traditional control of oxygen levels in cell culture is conducted using large hypoxic chambers at one concentration at a time.[10] Because of the large volume of air to be exchanged, hypoxic chambers are slow and cannot reach extreme levels of hypoxia. Several published microfluidic devices have improved this delivery by generating multiple oxygen concentrations simultaneously, then dissolving the concentrations in media perfusate that flows over target cells.[11–13] Alternatively, a gas impermeable flow chamber that allows an oxygen gradient to be generated *via* metabolic depletion of oxygen has been utilized to investigate oxygen gradients in culture, but this system was also under flow and its gradient profiles were limited to the cells utilized, due to the constant metabolic depletion rate for each given cell type.[14,15] Our previous work eliminated this flow and diffused oxygen through a thin membrane (100 μm), across 200 μm of media, to supply cells in standard multiwell plates.[16] In this report, an improved device directly diffuses oxygen to the cells seeded on top of a gas-permeable PDMS membrane as shown in Fig. 1. This eliminates the extra microfluidics required to control oxygen solvation in perfusates and removes the flow induced shear stress, which can itself trigger ROS production in the cells.[17] Additionally, by diffusing through the substrate, the volume of media available to the cells is no longer restricted as is the case with previous microfluidic oxygenation schemes and non-adherent cell types can be easily cultured in this platform. Using this direct diffusion, the device can provide faster and more localized delivery as shown in Fig. 1B, with equilibration occurring over seconds. We can provide these spatio-temporal oxygen controls similar to competing microfluidic devices without having to control the flow rate.[14,18] In comparison, our previous microfluidic add-on for multiwell plates equilibrated in minutes while standard hypoxic chambers required hours for equilibration.[16] As the gas is delivered from the bottom, the top of the device features a culturing reservoir, allowing standard culturing techniques that is both easy to handle and minimally invasive to the cells.

Department of Bioengineering, University of Illinois at Chicago, (MC063) 851 S. Morgan St 218 SEO, Chicago, IL, 60607, USA. E-mail: dte@uic.edu; Fax: +1 312-996-5921; Tel: +1 312-355-3278

† Published as part of a special issue dedicated to Emerging Investigators: Guest Editors: Aaron Wheeler and Amy Herr.

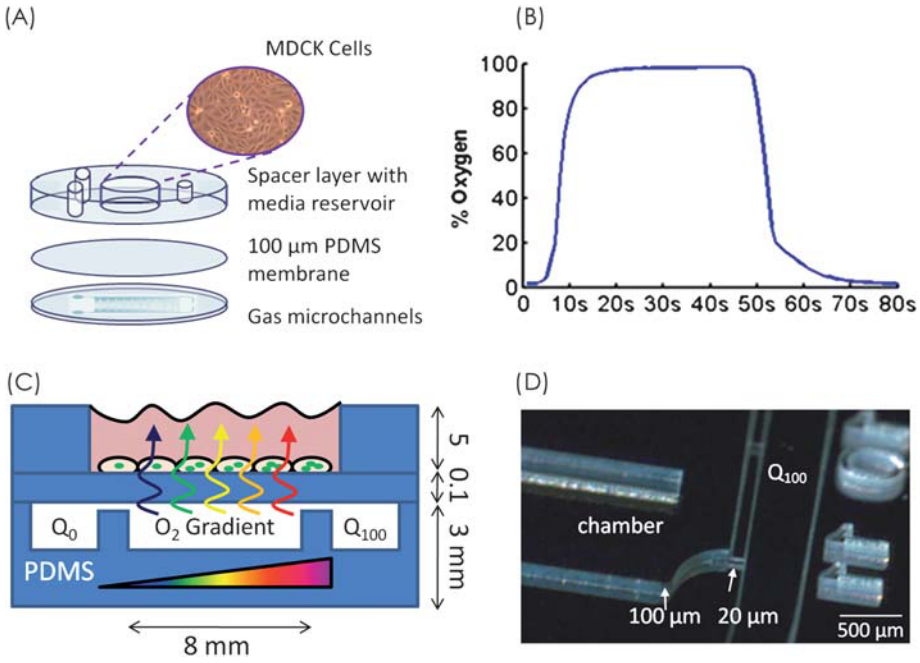

Fig. 1 Schematic of using microfluidic oxygen gradient to control culture cell ROS response. (A) Multi-layered devices consist of a gas microchannel layer, a 100 μm thick PDMS diffusion barrier, and a reservoir spacer layer for seeding MDCK cells. (B) Using diffusion based microfluidics, gas concentrations were rapidly exchanged and delivered (<20 s equilibrium) directly to the cells. (C) To deliver gas to the cells, a gradient (in this case the parallel flow design) was generated at the lower microfluidic layer by flowing a combination of 0 and 100% oxygen gases, Q_0 and Q_{100}, respectively. This O_2 gradient then diffused directly to the cells seeded above the 100 μm thick PDMS diffusion barrier. The high gas permeability of PDMS allows direct exposure of the seeded cells to oxygen levels, and their ROS production is monitored *via* intracellular fluorescent probe DCF (green dots). (D) SU8 mold around the Q_{100} channel shows thin 20 μm height channels connected to the rest of the 100 μm thick device, providing a diffusion-based gradient generation.

Using these cell culture friendly devices, two distinct oxygen profiles were applied to modulate the production of ROS in Madin–Darby Canine Kidney (MDCK) epithelial cells, covering both hyperoxic and hypoxic regimes of oxygen exposure. Both kidney cells at the organ level[19] and epithelial cell at the tissue level[20] are sensitive to ROS stress. This combination makes MDCK cells very relevant to ROS-related investigations. Their ROS levels were monitored *via* the intracellular fluorescent probe dichlorofluorescein diacetate (DCFDA). DCFDA, upon esterase cleavage of its diacetate moiety, is oxidized by H_2O_2 and peroxidases inside the cells, enabling its DCF moiety to fluoresce.[21] Furthermore, vitamin C was added as extrinsic supplement to enhance MDCK's intrinsic antioxidant regulation. Finally, oxygen modulated ROS response was compared to the standard method of inducing ROS in cellular cultures through application of hydrogen peroxide, to benchmark our device against the current standard method. These results provided an overview of oxidative events covering from hypoxia induced ROS to hyperoxia induced ROS cell damage and demonstrate the utility of the microfluidic oxygenation device.

2. Experimental

2.1 Parallel flow *versus* network mixer microgradient generator designs

To generate the oxygen microgradient, two microfluidic mechanisms were used: (1) diffusion between parallel channels as shown in Fig. 2A and (2) laminar mixing in bifurcating networked channels as shown in Fig. 2B. These structures have been demonstrated for liquid microfluidic devices,[22,23] but they have different properties with gas microfluidic devices. As gas has a much larger diffusion coefficient (2×10^{-5} m^2 s^{-1} oxygen diffusion[24] in air *vs.* 1×10^{-10} m^2 s^{-1} diffusion of typical dye, FITC, in water[25]), this enhances gas phase mixing and results in shorter channels required for the mixer network, but also higher flow rates in parallel channel structures (80 *vs.* 50 sccm in network mixer). Additionally, this also eliminates the classic step profile in liquid gradient networks and results in a smoothed profile, as seen in our data. Both the mixer and parallel flow devices were fed by 500 μm wide by 100 μm deep gas channels. For the parallel channel structure, a large diffusion chamber (8 mm wide) was connected between the parallel channels only by small 20 μm × 20 μm channels. Without reducing the diffusion to these 20 μm × 20 μm channels, open parallel flows of two gas concentrations would mix almost immediately. On the other hand, the improved mixing shortens the length of network mixer channels, providing multiple channels (eight 1 mm wide output channels) of concentrations as opposed to the continuous gradient across the parallel channel structure. As a result, devices fabricated using these two distinct mechanisms show distinct profiles for their oxygen microgradients. Slowing the flow rates injected in the network mixer could theoretically generate less steep profiles; and increasing the flow rate in the parallel flow device could conversely generate steeper profiles. However, we chose a single 0–150 sccm flow meter to ensure accurate control over ranges appropriate for both generators.

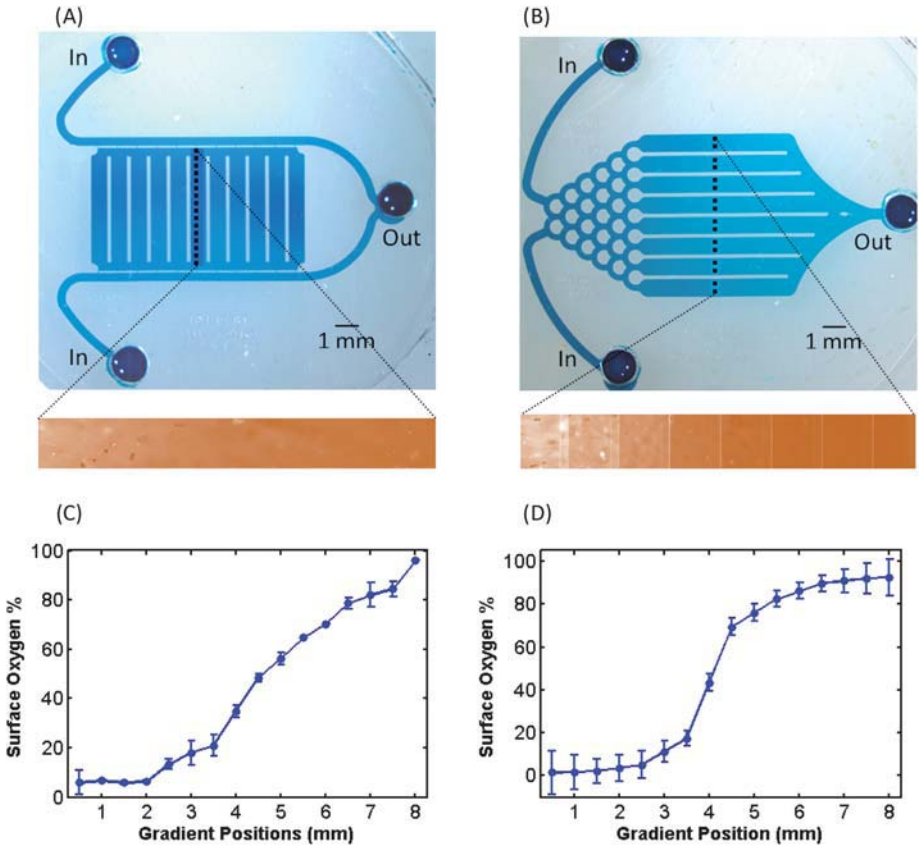

Fig. 2 Two microfluidic O_2 gradient generators. Devices using (A) diffusion between parallel flow channels and (B) mixing in network channels, generated distinct oxygen profiles. Inlet, outlets, and measurement positions (black dotted lines) were illustrated in photomicrographs of blue dye-filled devices. The chamber in the parallel flow device is supported by PDMS columns (white lines), and the gradient channels in the mixer device are separated also by PDMS columns. Oxygen gradient generated by the devices was imaged by the fluorescence quenching of the oxygen sensor (orange fluorescence imaged below the micrographs) with profiles that correspond to each device, shown by line scans in (C) and (D). Line scan profiles generated *via* (C) parallel channel device span more linearly than *via* (D) network mixing. The strong sigmoidal profile of the network mixer produces both strong hyperoxic and hypoxic conditions with O_2 down to 2%, compared to 7% for the parallel flow device. Error bars represent standard deviations from the mean.

2.2 Microgradient cell culture platform (MCCP) fabrication

The microfluidic gradient generators were integrated to a cell culture reservoir using standard polydimethylsiloxane soft lithography.[26] This integration created a device platform we named microgradient cell culture platform (MCCP). The MCCP integration was realized *via* a multilayered construction as shown in Fig. 1A, consisting of: (1) a bottom microfluidic channel, (2) a 100 μm PDMS thin film, and (3) a spacer layer with cell culture reservoir. First, microfluidic channels were patterned in SU8 resist using standard lithography. 100 μm thick SU8 was used for the main channels in both designs. However, the parallel flow design used additional two-layer lithography to integrate its 20 μm thick diffusion channels. Soft-lithography molding with this master forms the gas microfluidics bottom layer. Second, degassed PDMS is spun onto a silicon wafer at 900 rpm to form the 100 μm thin film diffusion layer. This thin film, punched with inlet/outlet ports, was bonded to the channel layer with 30 s of exposure from an ETP plasma surface treatment device (ETP, Inc). Third, a PDMS spacer layer punched with a 1 cm diameter media reservoir plus inlet/outlet ports was bonded to the previous two layers, forming the final multilayer sandwich for the MCCP. All microchannels were encapsulated by this spacer (~5 mm thick), except the gradient areas exposed for cell culturing. At their operating flow rates, there was no visible bubbling or bulging of the membrane even after 4 hours of operation.

2.3 Characterizing the oxygen microgradient

Prior to operating the MCCPs, they were validated for performance and generation of oxygen gradients. Upon fabrication, the devices were injected with gas and completely submerged in water to detect leaks. Then, the devices were measured by using an oxygen sensitive fluorescent probe—FOXY slide (Ocean Optics, Inc)—placed directly against the PDMS diffusion layer (refer to Oppegard *et al.* for detailed description[16]). Both devices were measured across 8 mm cross-sections of their gradients for comparison. Known oxygen concentrations of 0%, 21%, and 100% were first measured to calibrate for the FOXY probe at pre-recorded gradient positions in those cross-sections. Then, 0% and 100% oxygen were delivered to the device for gradient generation. The oxygen gradient-dependent fluorescence was measured at those pre-recorded positions.

2.4 MCCP cell seeding and ROS assay experiment

The ROS experiments were conducted with both parallel flow and network mixer MCCPs. The MCCPs were fabricated and characterized earlier and UV sterilized at 254 nm for 2 hours followed by incubation with 50 μM fibronectin for 2 hours to promote cell attachment onto the PDMS substrate. Adherent MDCK cells were grown to 90% confluency in standard culture flasks, then trypsinized with 0.25% trypsin in 0.53 mM ethylenediaminetetraacetic acid (EDTA) Hepes Buffered Saline Solution (HBSS) for 10 minutes in the incubator. The suspended cells were then seeded to the MCCPs at a concentration of 200 000 cells per mL in Dulbecco's Modified Eagle's Medium with serum and 1% penicillin–streptomycin (Pen–Strep). The seeded MCCPs were allowed to incubate overnight in a standard incubator. For experiments with vitamin C, the supplement was added to the media for the overnight incubation. Before the experiment, the cells were washed in phosphate buffer saline (PBS) and incubated with 3 μg mL^{-1} Hoechst DNA dye for 10 min, which prominently stains the cell nucleus. Then the cells were washed again, followed by incubation of 50 μM DCFDA ROS dye for 10 minutes. Staining seeded cells instead of suspended cells helped to minimize interferences from ROS generated during trypsinization. After loading the dyes, the cells were washed and maintained in PBS on a stage heated to 37 °C for the duration of the experiment. Gas was then delivered to the MCCPs and the ROS responses were measured *via* time-lapse microscopy for 2 hours at 20 minute capture intervals. At the end of the experiment, Trypan blue was incubated for the viability test. All assays were repeated at least three times to show consistency in measured responses with triplicate devices in each experiment.

2.5 Data analysis and ROS fold calculation

For the oxygen profile measurements, three separate experiments were conducted using three different devices each for both the parallel flow and network mixer designs. Similarly, the ROS response was measured in three separate experiments using different devices for both designs. The error bars for these experiments represented their respective standard deviations. Furthermore, the ROS responses were calibrated against their respective oxygen profiles, and then combined to show the overall trend *versus* oxygen concentration. Thus, it included data from six separate experiments, with error bars representing standard deviations. Finally, vitamin C response was also measured from three different experiments using both designs, with the error bars representing their standard deviations.

The ROS increase was calculated as "fold increase" in DCF intensity. The ROS fold increase is the ratio of the DCF fluorescence per cell at 2 hours (end of experiment) over time zero. Since the cells were co-stained with Hoechst (nucleus stain), we computed the DCF intensity per cell using a Metamorph script to count the cells by nucleus and report the average cell intensities. This accounted for the distribution of cells throughout the device as well as any changes in cell numbers (due to cell death, mobility, and detachment) within the 2 hour long experiment. The ratio, or ROS fold, thus represented the average increase of ROS-induced DCF intensity within one cell in a population of cells.

2.6 Hydrogen peroxide exposure comparison

The level of ROS production under oxygen exposure was compared to known concentrations of hydrogen peroxide exposure in MDCK cells. We chose to look at hydrogen peroxide, which readily diffuses across cell membranes, as the DCF dye is most sensitive to this radical species.[21] This comparison was conducted with hydrogen peroxide concentrations of 0 μM, 1 μM, 10 μM, 50 μM, 100 μM, 1 mM, and 2 mM in standard cell culture flasks. Cells were stained with Hoechst and DCF dyes while attached in the flask using exactly the same procedure described earlier for cells seeded on the MCCPs. Using hydrogen peroxide exposure, a quantitative comparison was done using the intracellular DCF dye, to investigate the concentration of oxygen radicals, mainly hydrogen peroxide, generated in the cell.

3. Results

3.1 Distinct oxygen profiles from two MCCPs

The two types of MCCP provided distinct gradients suitable for different oxygen exposure applications. The oxygen microgradient generated by the parallel channel MCCP showed a more linear profile than that from the network mixer MCCP, as shown in Fig. 2. The range of oxygen concentrations provided by the parallel channel MCCP was 7–97%. The network mixer generated a sigmoid-like profile, consistent with profiles reported in other network-based mixer.[22] While we aimed to provide binned (stepped) concentrations with our mixer, the steps were smoothed out by the faster cross-channel gas diffusion (5 orders magnitude[24,25,27]), compared to the diffusion of FITC dye used to characterize liquid phase mixers. 37 percent of the gradient (0–3 mm) was exposed to strong hypoxia (<10%) while 37 percent (5–8 mm) was exposed to strong hyperoxia (>80%). The device provided oxygen concentrations from 2–90%. While parallel MCCP provided oxygen profiles useful for looking at proportional responses of oxygen exposure, the profile from the network MCCP was better at targeting non-linear responses at extreme ends of the hypoxic/hyperoxic scale. These devices were operated over 0–100% oxygen levels, and these profiles would be similar in shape (linear or sigmoidal) with the upper and lower limits defined by the injected gases. For example, the device could be injected with 0 and 10% oxygen to explore this oxygen range in more detail. However we chose the 0–100% range to demonstrate the utility and full range possible with the device. In addition to the linear and sigmoidal profiles achieved in these devices, future modifications can be made to the channel flow[22] and resistances[28] to provide a number of distinct oxygen profiles.

3.2 ROS response modulated by oxygen microgradient profiles

Applying the two oxygen microgradient profiles to attached MDCK cells yielded different modulations of ROS responses as shown in Fig. 3. As the parallel channel MCCP has fairly linear oxygen profile, the ROS response turns out to be proportional. At the highest oxygen concentration, the parallel channel MCCPs induced the cells to pump out ROS levels that are 1.5 times more than the initial ROS reading at time zero. This "ROS fold" decreases linearly until it flattens out below 10%

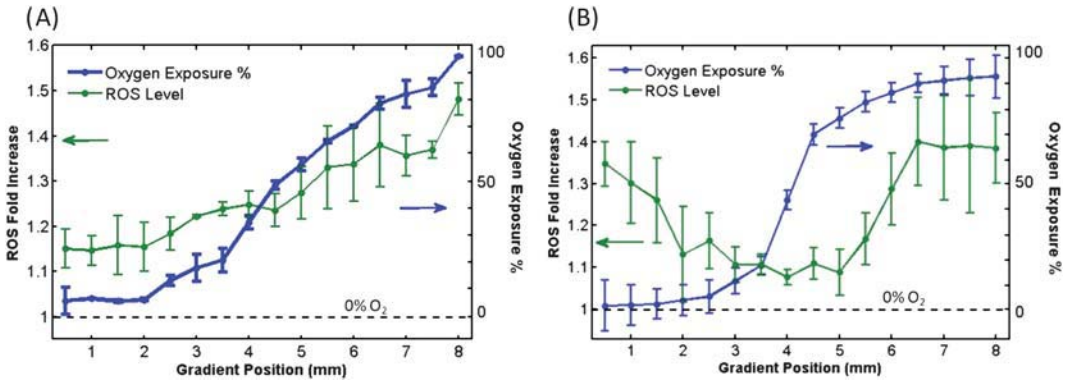

Fig. 3 Cell ROS response modulated by distinct profiles of oxygen exposure. Oxygen profile (blue) measured at an earlier time (from Fig. 2) is overlaid with ROS response (green) for both devices. (A) For parallel flow device, more linear oxygen profile (7–97% O_2) resulted in a proportional ROS response (1.15–1.5 folds) by the cells. (B) For the network mixer device, the steep sigmoidal oxygen profile (2–90% O_2) exposed cells to both hypoxia and hyperoxia, resulting in a v-shaped ROS profile (1.35 to 1.1 to 1.4 folds). Error bars represent standard deviations from the mean.

oxygen as shown in Fig. 3A. On the other hand, the ROS response from network mixer MCCPs resembled a v-shaped curve as shown in Fig. 3B. Both ends of the v-curve reached almost 1.4 fold ROS increase. Referring to earlier characterizations, the network mixer generated a stronger sigmoidal oxygen profile, as shown in Fig. 2. As part of the device was under deep hypoxia and part under hyperoxia, the ROS fold increased at both extremes. The lowest value the parallel channel mixer reached was 7% oxygen which helps explain why the hypoxic response was not apparent compared to the network mixer, which reached 2% oxygen. As a reference, 21% oxygen (standard cell culture concentration), present in both oxygen profiles, yielded 1.1–1.2 fold ROS increase, compared to the 1.4 and 1.5 achieved at the hypoxic and hyperoxic extremes, respectively.

3.3 Combined ROS responses *versus* antioxidants

When the ROS response from both parallel channel MCCPs and network MCCPs was analyzed and plotted against percent oxygen levels, Fig. 4A, all data show a consistent linear increase of ROS above 10%. Below 10%, hypoxia also induced an increase in ROS, most clearly illustrated in the network mixer MCCP data. The ROS increase at hypoxic conditions corroborates with published results of ROS involvement in HIF-1α stability,[6] while heightened ROS induced by hyperoxic exposure is also well documented in epithelial cells.[29–31] On the other hand, the cells that were incubated overnight with vitamin C showed no modulation of ROS across the range of oxygen levels, exhibiting the reported antioxidant benefits of the vitamin.[31] As a reference, the ROS increase at 21% oxygen with vitamin C is 1.1 fold. For all oxygen concentrations, no significant change in morphology or cytotoxicity was observed after two hours of exposure, as shown in Fig. 4B.

3.4 Hydrogen peroxide quantitation and cell morphology

The externally induced concentrations of hydrogen peroxide resulted in a positively correlated ROS response as shown in Fig. 5A. The ROS fold increase of 1.5 seen in MCCP oxygen exposures corresponds to hydrogen peroxide exposure concentrations below 100 μM. At these concentrations the cell morphology seen in fluorescent microscopy remains unchanged. At above 1 mM hydrogen peroxide concentration, however, cells begin to develop blebbing, a destructive phenomenon of

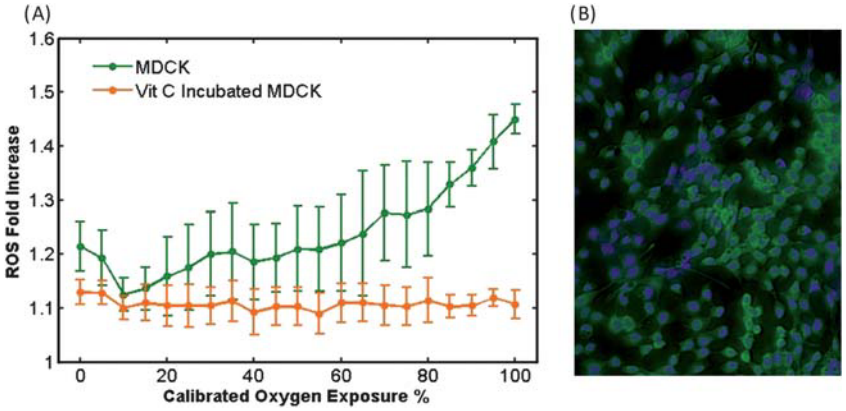

Fig. 4 Consistent cell ROS response yielded assays of oxidative damage *versus* vitamin fortification. (A) Graph: when compiled against oxygen exposure, both parallel and network mixer devices yielded similar ROS increase under hyperoxia. Consistently, ROS response changes at oxygen levels below 10%, leading to an increase under hypoxia. On the other hand, cells incubated with 200 μM vitamin C, an antioxidant, did not show an increase in ROS at any oxygen exposures. (B) Image: cell assayed in microfluidic gradient (2 h) saw no significant cell death (green: DCF; purple: Hoechst; gray: bright field overlay). Error bars represent standard deviations from the mean.

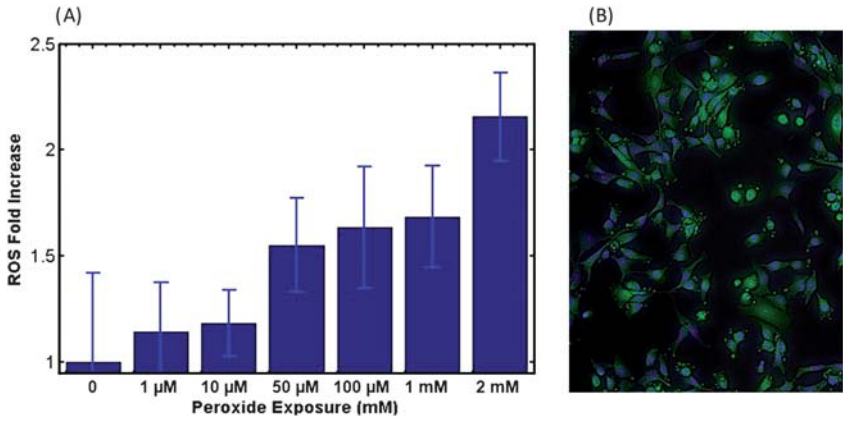

Fig. 5 Hydrogen peroxide exposure comparison. (A) Graph: hydrogen peroxide induced ROS signal from MDCK cells was recorded for concentrations 0–2 mM. Since the DCF dye is sensitive to hydrogen peroxide species of ROS, this comparison quantifies the amount of generated ROS. For ROS fold increase of 1–1.5, seen in O_2 exposure, the corresponding hydrogen peroxide range is 0–100 μM of H_2O_2. (B) Image: in hydrogen peroxide induced oxidative damage, 2 mM hydrogen peroxide is able to rapidly induced blebbing, a late stage event in apoptosis, leading to high cell death. Error bars represent standard deviations from the mean.

post-apoptotic kinase activity that results in bubbling of the cell membranes and cell disintegration as shown in Fig. 5B. This is not seen from the cells in MCCP devices as shown in Fig. 4B. Despite this, H_2O_2 remains the method of choice for ROS induction in cellular models up to mM range.[32] However, our device can achieve the same results through intrinsic mechanisms without the addition of chemicals.

4. Discussion

Due to the distinct oxygen profiles of the two MCCPs, hypoxic and hyperoxic modulations of ROS were demonstrated. Linear profile from the parallel MCCP device favored a proportional way of looking at hyperoxia induced ROS. On the other hand, the sigmoidal profile from the network mixer MCCP emphasized the extremes of hypoxia and hyperoxia. Furthermore, these profiles can be focused onto narrower ranges of concentrations. For example when investigating hypoxic conditions researchers could select a midpoint of expected response, such as 5%, and run the device from 0–10%. The linear profile could be useful for developing a biomimetic model of certain phenomena, while the sigmoidal profile could stretch the extremes flanking a midpoint to investigate which O_2 level triggers a given phenomena of interest. In addition, the use of antioxidant vitamin C, or any other ROS scavenging/neutralizing factors, can enable ROS-free investigation of other oxygen-dependent pathways.[33,34] To support the quantitation of MCCP results, the comparative hydrogen peroxide exposure assay provided a much needed concentration scale upon which to compare the time-changing ROS modulations. Although hydrogen peroxide is the gold standard for inducing ROS signaling in cell cultures, our device is able to achieve similar ROS levels with a more physiologically relevant method of induction. Additionally, hydrogen peroxide is a short lived molecule. Spontaneous decomposition, reaction with metal ions, and UV–ozone interaction deplete the species in complex extracellular media environments,[35,36] leading to a shortened period of induction. On the other hand our oxygen exposure platform is able to constantly induce ROS responses, which in and of itself is a major advance over the current methods. However, future experiments can benefit from dyes like dihydroethidium (DHE) which are specific to superoxides, instead of the broadly reactive DCF,[21] to enable more detailed time-lapse monitoring of ROS species.

The results from the ROS assay illustrated the physiological process of oxidative stress in cultured cells. We observed an increase in ROS at higher oxygen exposures as shown in Fig. 4. This observed relationship was expected and a consequence of increased respiration.[37] Especially in epithelial and kidney cells like MDCK, overactive mitochondrial metabolism *via* NADPH oxidase produces the majority of the ROS increase that damages cells during oxidative stress.[37] In the other extreme, data below 10% oxygen also showed an increase in ROS under hypoxia, with ROS–HIF-1α interactions attributed to this phenomenon as expected.[6] Both strong hypoxic and hyperoxic exposures produced ROS increases and required an additional 200 μM vitamin C to demodulate their ROS responses, as shown in Fig. 4. As a note to the utility of vitamin C, the cultures could be exposed to hyperoxic or hypoxic conditions without ROS present to examine the role oxygen plays in cellular signaling pathways in the absence of ROS.

In addition to ROS responses, cell viability test for MCCP devices showed no dramatic changes in cell death at both extremes of oxygen exposure as shown in Fig. 6. This meant that for the hypoxic and hyperoxic mechanisms described above, their ROS production, at levels corresponding to intracellular signaling, had not yet reached the destructive end of cell toxicity. The higher ROS increase from 2 mM hydrogen peroxide exposure, on the other hand, represented a cut-off point where cell signaling changes into apoptotic programming as shown by the image in Fig. 5.

Future iterations could leverage previously demonstrated techniques to tailor fit the device to niche applications. For instance, cells could be micropatterned onto the membrane to further define the microenvironment.[38] Cells could also be confined into discreet regions without cell–cell junctions by microwells on the substrate.[39] Additionally, instead of gradients,

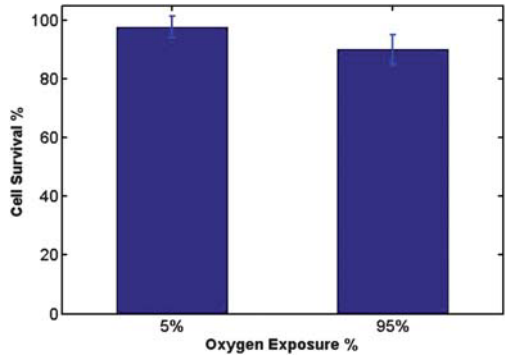

Fig. 6 Over 90% cell survival achieved for low and high oxygen in MCCPs (2 h). Survival was investigated with Trypan blue incubation. Cells under 5 and 95% oxygen exposure observed less than 10% death in MCCP devices. Error bars represent standard deviations from the mean.

entire cultures could also be exposed to single oxygen concentrations by running the same gas composition through both inlets. All of these future possibilities would be dependent on PDMS based membranes due to its excellent oxygen diffusivity, and future iterations could also implement techniques to reduce PDMS absorption of hydrophobic small molecules.[40]

Notably, this oxygen exposure based ROS study would have been difficult to carry out in other types of devices. Many types of oxygenation devices depend on media perfusion over channel encapsulated cells, producing pressure and shear stress that themselves induce background ROS unrelated to oxygen exposures.[17,41] In addition, the elimination of gas solvation removes bubbling and advection/drying problems. Moreover, scientists who focus on the biology of their experiments, rather than the methods and instruments, would appreciate the reduction of parameters that might influence cell response, especially for maintaining a reproducible, cell-friendly microenvironment. Because of the gentle handling of the cells and compatibility with standard cell culture techniques, MCCP devices provide a much needed tool for microscopy based oxygen exposure studies. As oxygen and oxidative mechanisms are pervasive in numerous cell signaling, molecular modification, growth, and tissue healing pathways, MCCP devices can be a common platform to standardize microgradient oxygen assays.

5. Conclusion

With microgradient integrated cell culture platforms, two distinct oxygen profiles were applied to modulate MDCK cell ROS levels. The parallel flow MCCP induced a linear oxygen profile while the network mixer MCCP induced a steep sigmoidal oxygen profile. The ranges of concentrations were 7–97% and 2–90% for the parallel and network mixer MCCPs, respectively. Because of the difference in oxygen ranges and their profile shapes, ROS responses ranged from a linear trend to v-shaped curve for parallel *vs.* network mixer MCCPs, respectively. When tabulated against the percent oxygen exposure, both MCCPs produced consistent, linear increases in ROS above 10% oxygen. Below 10% oxygen the strong hypoxia exerted by the network mixer MCCP produced an ROS increase that is reportedly associated with HIF-1α interactions. 200 μM vitamin C were able to counteract both hypoxic and hyperoxic ROS increases, at levels corresponding to 100 μM hydrogen peroxide concentration, the major species detected by intracellular DCF dye. The MCCP oxygen assay provided a complete range of exposure studies while allowing quantification *via* measure ROS fold increase.

Acknowledgements

This work was supported by the Multidisciplinary Oral Sciences Training Program, National Institutes of Health Grant T32 DE018381-01 and NSF 0852416.

References

1 J. T. Erler, K. L. Bennewith, N. Dornhoefer, M. Nicolau, J. T. A. Chi, S. S. Jeffrey and A. J. Giaccia, *Nature*, 2006, **440**, 1222–1226.
2 C. K. Sen, *Wound Repair Regener.*, 2009, **17**, 1–18.
3 H. K. Said, J. Hijjawi, N. Roy, J. Mogford and T. Mustoe, *Arch. Surg. (Chicago, IL, U. S.)*, 2005, **140**(10), 998–1004.
4 C. Dennog, et al., *Mutat. Res., Fundam. Mol. Mech. Mutagen.*, 1999, **431**(2), 351–359.
5 C. W. Pugh and P. J. Ratcliffe, *Nat. Med. (Tokyo, Jpn.)*, 2003, **9**, 677–684.
6 R. D. Guzy, B. Hoyos, E. Robin, H. Chen, L. Liu, K. D. Mansfield, M. C. Simon, U. Hammerling and P. T. Schumacker, *Cell Metab.*, 2005, **1**(6), 401–408.
7 T. Finkel and N. J. Holbrook, *Nature*, 2000, **409**, 239–247.
8 K. Zhang and R. J. Kaufman, *Nature*, 2008, **454**, 455–462.
9 C. Li and R. M. Jackson, *Am. J. Physiol. Cell Physiol.*, 2002, **282**, C227–C241.
10 C. B. Allen, B. K. Schneider and C. W. White, *Am. J. Physiol. Lung Cell Mol. Physiol.*, 2001, **281**, L1021–L1027.
11 B. J. Kane, M. J. Zinner, M. L. Yarmush and M. Toner, *Anal. Chem.*, 2006, **78**, 4291–4298.
12 R. H. W. Lam, M. C. Kim and T. Thorsen, *Anal. Chem.*, 2009, **81**, 5918–5924.
13 M. Polinkovsky, E. Gutierrez, A. Levchenko and A. Groisman, *Lab Chip*, 2009, **9**, 1073–1084.
14 J. Allen and S. N. Bhatia, *Biotechnol. Bioeng.*, 2003, **82**(3), 253–256.
15 G. Mehta, K. Mehta, D. Sud, J. W. Song, T. Bersano-Begey, N. Futai, Y. S. Heo, M. A. Mycek, J. J. LInderman and S. Takayama, *Biomed. Microdevices*, 2007, **9**(2), 123–134.
16 S. C. Oppegard, K. H. Nam, J. R. Carr, S. C. Skaalure and D. T. Eddington, *PLoS One*, 2009, **4**(9), e6891.
17 H. J. Hsieh, C. C. Cheng, S. T. Wu, J. J. Chiu, B. S. Wung and D. L. Wang, *J. Cell. Physiol.*, 1998, **175**(2), 156–162.
18 M. Adler, M. Polinkovsky, E. Gutierrez and A. Groisman, *Lab Chip*, 2010, **10**, 388–391.
19 N. D. Vaziri, M. Dicus, N. D Ho, L. Boroujerdi-Rad and R. K. Sindhu, *Kidney Int.*, 2003, **63**, 179–185.
20 F. D. Khand, M. P. Gordge, W. G. Robertson, A. A. Noronha-Duttra and J. S. Hothersall, *Free Radical Biol. Med.*, 2002, **32**(12), 1339–1350.
21 W. O. Carter, P. K. Narayanan and J. P. Robinson, *J. Leukocyte Biol.*, 1994, **55**(2), 253–258.
22 W. N. L. Jeon, S. K. W. Dertinger, D. T. Chiu, I. S. Choi, A. D. Stroock and G. Whitesides, *Langmuir*, 2000, **16**, 8311–8316.
23 S. Paliwal, P. A. Iglesias, K. Campbell, Z. Hilioti, A. Groisamn and A. Levchenko, *Nature*, 2007, **446**, 46–51.
24 J. R. Welty, C. E. Wicks and R. E. Wilson in *Fundamentals of Momentum, Heat, and Mass Transfer*, John Wiley & Sons, NY, 3rd edn, 1984, p. 803.
25 P. Galambos and F. K. Forster, *Micro Total Anal. Syst.*, 1998, 189–192.
26 D. C. Duffy, C. McDonald, O. J. A. Schueller and G. M. Whitesides, *Anal. Chem.*, 1998, **70**, 4974–4984.
27 P. Han and D. M. Bartels, *J. Phys. Chem.*, 1996, **100**, 5597–5602.
28 D. Irimia, D. A. Geba and M. Toner, *Anal. Chem.*, 2006, **78**, 3472–3477.

29 T. E. Zaher, E. J. Miller, D. M. P. Morrow, M. Javdan and L. L. Mantell, *Free Radicals Biol. Med.*, 2007, **42**(7), 8908.
30 S. R. Khan, *Urol. Res.*, 2005, **33**, 349–357.
31 H. Jyonouchi, S. Sun, M. Mizokami and D. H. Ingbar, *J. Allergy Clin. Immunol.*, 1996, **97**(1), 538.
32 A. Domont, S. P. Hehner, T. G. Hoffmann, M. Ueffing, W. Dröge and L. Schmitz, *Oncogene*, 1999, **18**, 747–757.
33 S. Roy, et al., *Circ. Res.*, 2003, **92**, 264–271.
34 G. R. S. Budinger, M. Tso, D. McClintock, D. A. Dean, J. J. Sznajder and N. Chandel, *J. Biol. Chem.*, 2002, **277**, 15654–15660.
35 J. Staehelin and J. Holgne, *Environ. Sci. Technol.*, 1982, **16**, 676–681.
36 D. P. Nelson and L. A. Kiesow, *Anal. Biochem.*, 1972, **49**, 474–478.
37 P. J. Lee and A. M. K. Choi, *Free Radical Biol. Med.*, 2003, **35**(4), 341–350.
38 D. Falconnet, G. Csucs, H. M. Grandin and M. Textor, *Biomaterials*, 2006, **27**(16), 3044–3063.
39 A. Khademhosseini, J. Yeh, G. Eng, J. Karp, H. Kaji, J. Borenstein, O. C. Farokhzad and R. Langer, *Lab Chip*, 2005, **5**, 1380–1386.
40 A. R. Abate, D. Lee, T. Do, C. Holtze and D. A. Weitz, *Lab Chip*, 2008, **8**, 516–518.
41 E. J. Belin de Chantemèle, E. Vessières, O. Dumont, A. L. Guihot, B. Toutain, L. Loufrani and D. Henrion, *Microcirculation*, 2009, **16**(5), 391–402.